

Caenorhabditis elegans RAC1/ced-10 mutants as a new animal model to study very early stages of Parkinson's disease

A. Muñoz-Juan^a, N. Benseny-Cases^b, S. Guha^c, I. Barba^d, K.A. Caldwell^{e,f}, G.A. Caldwell^{e,f}, L. Agulló^d, V.J. Yuste^{g,1}, A. Laromaine^{a,1}, E. Dalfó^{d,g,h,*,1}

^a Group of Nanoparticles and Nanocomposites, Institut Ciència de Materials de Barcelona, ICMAB-CSIC, Campus UAB, 08193 Bellaterra, Barcelona, Spain

^b Biophysics Unit. Department of Biochemistry and Molecular Biology. Universitat Autònoma de Barcelona, Bellaterra 08193, Barcelona, Spain

^c Nautilus Biotechnology, 835 Industrial Rd, San Carlos, CA 94070, USA

^d Faculty of Medicine, University of Vic-Central University of Catalonia (UVic-UCC), Institute for Research and Innovation in Life Sciences and Health in Central Catalonia (IRIS-CC), Can Baumann, 08500 Vic, Spain

^e Department of Biological Sciences, The University of Alabama, Tuscaloosa, AL 35487, USA

^f Department of Neurology, Center for Neurodegeneration and Experimental Therapeutics, and Nathan Shock Center of Excellence in the Basic Biology of Aging, University of Alabama at Birmingham Heersink School of Medicine, Birmingham, AL 35294, USA

^g Department of Biochemistry and Molecular Biology, Institut de Neurociències, Faculty of Medicine, M2, Universitat Autònoma de Barcelona (UAB), Bellaterra Campus, Cerdanyola del Vallès, Barcelona, Spain

^h Institute of Neurosciences, Faculty of Medicine, Universitat Autònoma de Barcelona (UAB), Campus UAB, 08193 Cerdanyola del Vallès, Spain

ARTICLE INFO

Keywords:

Early-Parkinson's disease
Early diagnosis RAC1/ced-10 nematodes
Lipid metabolism
GABAergic impairment

ABSTRACT

Patients with Parkinson's disease (PD) display non-motor symptoms arising prior to the appearance of motor signs and before a clear diagnosis. Motor and non-motor symptoms correlate with progressive deposition of the protein alpha-synuclein (Asyn) both within and outside of the central nervous system, and its accumulation parallels neurodegeneration. The genome of *Caenorhabditis elegans* does not encode a homolog of Asyn, thus rendering this nematode an invaluable system with which to investigate PD-related mechanisms in the absence of interference from endogenous Asyn aggregation. CED-10 is the nematode homolog of human RAC1, a small GTPase needed to maintain the function and survival of dopaminergic neurons against human Asyn-induced toxicity in *C. elegans*. Here, we introduce *C. elegans* RAC1/ced-10 mutants as a predictive tool to investigate early PD symptoms before neurodegeneration occurs. Deep phenotyping of these animals reveals that, early in development, they displayed altered defecation cycles, GABAergic abnormalities and an increased oxidation index. Moreover, they exhibited altered lipid metabolism evidenced by the accumulation of lipid droplets. Lipidomic fingerprinting indicates that phosphatidylcholine and sphingomyelin, but not phosphatidylethanolamine or phosphatidylserine, were elevated in RAC1/ced-10 mutant nematodes. These collective characteristics reflect the non-motor dysfunction, GABAergic neurotransmission defects, upregulation of stress response mechanisms, and metabolic changes associated with early-onset PD. Thus, we put forward an easy-to-manipulate preclinical animal model to deepen our understanding of early-stage PD and accelerate the translational path for therapeutic target discovery.

1. Introduction

Parkinson's disease (PD) is the second most common neurodegenerative disorder after Alzheimer's and has become one of the leading causes of disability worldwide (Feigin et al., 2017). The clinical

diagnosis of PD is based on motor symptoms, which can appear between three and six years after the onset of neuronal degeneration entailing the depletion of 60–80% of the brain's dopaminergic neurons (Gaig and Tolosa, 2009). Besides the motor symptoms, PD patients also show disturbances in the autonomic non-motor system arising during early

* Correspondence to: Institut de Neurociències, Faculty of Medicine (Edifici M-1), Carrer de la Vinya, Bellaterra Campus, 08193 Cerdanyola del Vallès, Barcelona, Spain.

E-mail addresses: esther.dalfo@uab.cat, estherdalfo@gmail.com (E. Dalfó).

¹ Co-senior author.

<https://doi.org/10.1016/j.pneurobio.2024.102572>

Received 31 July 2023; Received in revised form 21 November 2023; Accepted 15 January 2024

Available online 20 January 2024

0301-0082/© 2024 The Authors. Published by Elsevier Ltd. This is an open access article under the CC BY license (<http://creativecommons.org/licenses/by/4.0/>).

phases, and often predating the motor manifestations. Constipation is the most prevalent non-motor symptom, which is often coincident with anxiety and Rapid Eye Movement (REM) sleeping behavior (Camerucci et al., 2023). Both motor and non-motor symptoms correlate with the progressive accumulation of the protein alpha-synuclein (Asyn) in the brain as part of proteinaceous structures named Lewy bodies, which are implicated in PD pathophysiology (Winner et al., 2011). For this reason, PD is considered a proteinopathy (Fanning et al., 2020). In addition, lipid accumulation leads to increased lipid peroxidation products that are neuropathological hallmarks of different synucleinopathies, damaging different brain structures (Dalfó and Ferrer, 2008). Thus, for this, PD is also considered a lipidopathy (Fanning et al., 2020).

Altered unsaturated lipids underlie PD in affected brains (Fu et al., 2022), and plasma polyunsaturated fatty acid (PUFA) levels are abnormal at the early stages of the disease, independent of food intake (15). The abundance of unsaturated lipids increases susceptibility to lipid peroxidation, a process of oxidative degradation of cellular lipids which is an important factor in the pathogenesis of neurodegenerative diseases. In particular, patients with early stages of Parkinsonian neuropathology showed elevated indicators of lipoxidative damage in the *Substantia nigra*, amygdala, and frontal cortex, compared with age-matched controls (Dalfó and Ferrer, 2008).

Caenorhabditis elegans (*C. elegans*) has been established as an important model organism for neuroscientific research (reviewed in (Roussos et al., 2023)). Many molecules involved in neuronal signaling and metabolism are conserved between nematodes and humans, and *C. elegans* experimental models have been predictive of results for human diseases (Roussos et al., 2023; Coppa et al., 2020). In the case of PD, two *C. elegans* models have been widely employed to investigate dopaminergic neuronal death (strain UA196) and Asyn accumulation (strain NL5901). Both, dopaminergic loss and Asyn aggregates ameliorate after overexpression of CED-10, the *C. elegans* homolog to human *RAC1* (Kim et al., 2018). For this reason, worms with a non-null altered function mutation in *ced-10* has also been successfully employed to investigate PD (Kim et al., 2018). The *C. elegans* genome does not contain an ortholog of Asyn, which makes the nematode an invaluable organism for investigating Asyn-related pathologies (synucleinopathies), such as PD, without the influence of endogenous Asyn expression. Still, transgenic strains of *C. elegans* expressing human Asyn from a multicopy transgene array recapitulate the progressive, age-dependent dopaminergic neurodegeneration observed in PD.

RAC1/CED-10 is a small GTPase controlling cytoskeletal dynamics (Hall and Lalli, 2010) and its activity is mainly associated with cellular processes involving the regulation of actin polymerization such as cell migration, lamellipodia extension or phagocytosis of dead cells (Kinchen et al., 2005). Hence, alterations in *RAC1* activity have been involved in a wide range of cellular mechanisms, such as governing changes in neuronal morphology (Banka et al., 2022).

Here, we show that *RAC1/ced-10* mutant nematodes display early developmental alterations in GABAergic axons and altered defecation behavior. In addition, these mutants display lipid alterations such as an increase in the amount of lipid droplets (LD) amount and in the lipoxidation index, and an altered lipidome fingerprint. These same phenotypes are also characteristic of patients with incidental causes of idiopathic PD. Therefore, we explore the suitability of *RAC1/ced-10* mutants as a new model for the investigation of the early stages (of PD and related synucleinopathies).

2. Materials and methods

2.1. *C. elegans* strains

Nematodes were maintained using standard procedures (Brenner, 1974). The information about the strains used in this study is summarized in Supplementary Table 1.

We obtained the strains NL5901 (named Asyn::YFP in the main

manuscript), *unc-119(ed3) III*; [*pkIs2386* (*Punc-54::α-SYN::YFP*; *unc-119* (+))], CZ1200 *juls76* [*Punc-25::GFP*], SJ4005, *zcls4 V* [*hsp-4::GFP*] and SJ4100, *zcls13 V* [*Phsp-6::GFP* + *lin-15(+)*] from the *Caenorhabditis elegans* Genetic Center (CGC). The strain BR3579, *ced-10(n3246)*, named *rac1/ced-10* in the main manuscript, was a generous gift from Dr. Ralf Baumeister (Albert-Ludwing University, Freiburg/Breisgau, Germany).

The strain BR3579 was crossed with NL5901 animals to generate the strain EDC101, *unc-119(ed3) III*; [*pkIs2386* (*Punc-54::α-SYN::YFP*; *unc-119* (+))]; *ced-10(n3246)* (Kim et al., 2018) (Sup. Fig. S1).

The strain used for rescuing Asyn aggregation was named UA282 and genotyped *baEx167* [*Pced-10::CFP::ced-10*; *rol-6(su1006)*]; *sid-1(pk3321)*; *baln33* [*Pdat-1::sid-1*, *Pmyo-2::mCherry*]; *baln11* [*Pdat-1::α-SYN*; *Pdat-1::GFP*]. The generation of these rescue strains was widely described in (Kim et al., 2018).

To analyze the axonal damage, males from the strain CZ1200 were crossed with *ced-10(n3246)* hermaphrodites to generate the strain EDC073, genotyped *juls76* [*Punc-25::GFP*]; *ced-10(n3246)* (Sup. Fig. S1).

N2 (Bristol) was used as the *C. elegans* wild-type (wt) strain. Hermaphrodites were used throughout of the study.

2.2. Worm culture and maintenance

Worms were cultured and maintained at 22 °C on standard nematode growth media (NGM) seeded with *E. coli* OP50 bacteria. Worm synchronization was carried out using a standard protocol as previously described (Stiernagle, 2006). In brief, gravid hermaphrodites were collected by washing them off the NGM plates and reconstituted to total 3.5 ml using M9 buffer. The worm solution was mixed with a fresh mixture of 0.5 ml 10 N NaOH and 1 ml bleach to achieve a complete release of eggs from the worm body through a repeated shaking-and-vortexing step every 2 min for a total of 8–10 min. The eggs were washed by M9 for five times and then seeded onto NGM plates with proper density. The L4 stage was verified by visual inspection under a microscope and collected at 47–48 h after egg treatment at 20 °C. We observed that *rac1/ced-10* mutant nematodes showed developmental defects. This fact implied a delay of approximately 12 h compared to wild-type to reach the L4 larval stage.

For lipidomic analysis, samples were collected and processed by the former company Biópolis, now part of the ADM company (<https://www.adm.com/>). 90 plates were collected wild types and 150 plates for the *RAC1/ced-10* mutant worms to achieve 100 mg of dried pellet per strain. Considering the hatching defects displayed by *RAC1/ced-10* mutant worms, the number of plates was increased to obtain the same biomass. The harvested worms were stored at −80 °C until use.

2.3. Blinding of experiments and replicates

All behavioral experiments were carried out with the experimenter being blind of the worms' genotype. Another lab member assigned letter codes to the strains, and the code was not revealed until all the duplicates for a particular assay were finished. We carried out a minimum of three biological replicates of each assay per strain.

2.4. Visualization of engulfment defects

Unengulfed apoptotic cell corpses were visualized directly in the heads of young larvae (L1) as refractile disks using Nomarski differential interference contrast (DIC) microscopy (Leica DM 6000 microscope) (Cabello et al., 2014).

2.5. Aggregate quantification

The quantification of aggregates was performed as previously described (Kim et al., 2018), (Van Ham et al., 2008). Briefly, NL5901 animals without and with *ced-10(n3246)* mutation and at the

indicated developmental stage, together with the EDC101 and the rescue strain, were age-synchronized by bleaching with NaOCl and left overnight to hatch. L1 animals were transferred onto individual NGM plates seeded with *Escherichia coli*. Aggregates were counted for each animal staged at L1 and L4, separately. Images were captured using a Leica SP5 confocal microscope with a $\times 40$ oil immersion lens (HCX PL APO CS). The number of Asyn aggregates was determined in the head of each animal. Aggregates were defined as discrete, bright structures, with boundaries distinguishable from surrounding fluorescence. Measurements on inclusions were performed using ImageJ software taking into consideration the area dimensions.

2.6. Thrashing assay

The repetitive pattern of activity known as thrashing involves the worm oscillating side to side around its midline. A thrash is the movement through the middle and back. The thrashing assay was performed blindly and in liquid medium as described previously (Coppa et al., 2020). A drop of 2% agarose was poured over the glass slide and allowed to dry. After adding 20 μ l of M9, L4 synchronized animals were placed on the drop and left for 2 min. Thrashes were counted for 30 s, and every animal was counted three consecutive times to obtain an average. This value was multiplied by two to obtain an estimate per minute. A single thrash was defined as a complete change in the direction of the body down the midline. Animals who were motionless for 10 s were discarded from the analysis.

2.7. Quantification of GABAergic-associated abnormalities

Worms were grown at 20 °C for at least two generations before the experiments. Animals were transferred daily to avoid mixing populations. After synchronization, F1 hermaphrodite animals were maintained at 20 °C until reaching L4 larval stage.

On the actual day of the experiment, worms at L4 were washed, anaesthetized in 10 mM sodium azide on 6% agar pads and subsequently mounted for image analysis. The worms were scored for the number of GABAergic neurons, gaps in the ventral cord, gaps in the dorsal cord and defects in axonal morphology (Coppa et al., 2020). The applied formula used to quantify axonal damage is: % of axonal damage = [(number of commissural abnormalities + number of gaps/animal)/number of axons detected] $\times 100$. The experiment was performed blindly and by different investigators to guarantee the reliability of the obtained measurements.

2.8. Synchrotron radiation μ fourier-transform infrared spectroscopy (SR- μ FTIR)

L3 worms were grown in NGM plates with OP50 at 20 °C. Several washing steps with MQ water were performed to remove the excess of OP50 and salts that could interfere with the measurements. Cleaned worms were transferred to a CaF2 window and dried at RT in vacuum conditions for 24 h. Samples were maintained in vacuum conditions and 4 °C until they were measured. For SR- μ FTIR data acquisition a Hyperion 3000 Microscope coupled to a Vertex 80 spectrometer (Bruker, Billerica, MA) equipped with 36x magnification objective was used at MIRAS beamline at Synchrotron ALBA (Cerdanyola del Vallés, Barcelona, Spain). The spectra collection was performed in transmission mode at 4 cm⁻¹ spectral resolution, 8 \times 8 μ m aperture dimensions using a MCT detector. For each spectrum, 128 scans were co-added, and the measuring range was 900–4000 cm⁻¹. FTIR spectra were acquired in 10 worms of each type at different locations of the worm (from head to tail with an average of 6 points per worm).

SR- μ FTIR data was analyzed using OPUS 7.5 (Bruker), Unscrambler X 10.5, MATLAB R2010b, and GraphPad Prism 9 version. Spectra presenting high RMies scattering, that usually appears in biological samples, were eliminated, and the rest of the spectra were corrected using a

mathematical algorithm described by (Bassan et al., 2010). For data analysis the second derivative of the spectra (Savitsky-Golay algorithm, 13-point filter, and polynomial order of two) was calculated to avoid baseline contribution and to improve the band resolution (Benseny-Cases et al., 2014). In this project, we studied lipid oxidation in wild-type and *RAC1/ced-10 C. elegans*. The carboxyl group (-COOH) has a characteristic absorption band at 1740 cm⁻¹ that has been normalized by the addition of the intensities of the methylene group (-CH2) absorption band at 2920 cm⁻¹ and the methyl group (-CH3) absorption band as a reference for lipids in worms (Benseny-Cases et al., 2014) in order to compare between the two strains.

2.9. Oil red O staining

Oil red O stock solution (5 mg ORO/ml Isopropanol) is diluted to 60% with distilled water and filtered with 0.22 μ m filter to obtain ORO work solution. Young adult worms were cleaned with M9 and fixed 15 min in a 50% isopropanol solution. Fixed worms were centrifuged at 7000 rpm for 1 min and the supernatant was replaced by 900 μ l of ORO work solution. After 17 h at RT in a rocking movement, stained worms were cleaned with three rounds of PBS and three rounds PBST (0.01% TritonX). Each round consists of 2 min-centrifugation at 7000 rpm and replacing the supernatant with fresh solution. Worms were mounted in 2% agarose pads and images were taken in the same light exposure conditions. Images were obtained with the microscope Olympus RXSITRF 52787 MAB INDUSTRIAL and the intensity of the stain was evaluated using the ImageJ-Fiji software. Each assay was performed in triplicate. Unpaired t-test within a confidence level of 95% was performed using Graphpad prism 9 version.

2.10. Microscopy and imaging

Microscopy and imaging are described differently for each experiment in the corresponding section.

For mitochondrial stress response (mtUPR) and unfolded protein response (UPR) measurements, animals were placed in a 5 μ l drop of 10 mM solution of levamisole (Sigma-Aldrich, Madrid, Spain). For each independent experiment, between 20 and 30 L4 worms of each strain were examined under a Nikon EclipseTE2000-E epifluorescence microscope equipped with a monochrome camera (Hamamatsu ORCA-ER) coupled to the Metamorph software (Molecular Devices Corp., Sunnyvale, CA). The system acquires a series of frames at specific Z-axis position (focal plane) using a Z-axis motor device.

2.11. Lipidomic profiling

The lipid profile was obtained from the analysis performed by OWL-metabolomics (<https://owlmetabolomics.com/>) and based on the lipidomic platform number 2 (complex lipids diacylglycerides, triacylglycerides, sphingolipids and glycerophospholipids; following the protocol described in (Martínez-Arranz et al., 2015). Briefly, lipids were extracted using a two-step chloroform/methanol procedure (Ejlsing et al., 2009). Dried extracts were reconstituted in acetonitrile / isopropanol (1:1), resuspended for 10 min, centrifuged (16,000 \times g for 5 min), and transferred to vials for UHPLC-MS analysis that was done as described (Martínez-Arranz et al., 2015).

SM (d18:1/6:0), PE (17:0/17:0), PC (19:0/19:0), TAG (13:0/13:0/13:0), TAG (17:0/17:0/17:0), Cer (d18:1/17:0) and ChoE (12:0) were considered as internal standards and used for internal response correction. Additionally, two different types of quality control (QC) samples were used to assess the data quality (Martínez-Arranz et al., 2015). The QC samples are reference serum samples, which are evenly distributed over the batches and extracted and analyzed at the same time as the individual samples. QC Calibration sample were used to correct the different response factors between and within batches. QC Validation sample were used to assess how well data pre-processing procedure

improved the data quality. Randomized sample injections were performed, with each of the QC calibration and validation extracts uniformly interspersed throughout the entire batch run.

All data were processed using the TargetLynx application manager for MassLynx 4.1 software (Waters Corp., Milford, USA). A set of pre-defined retention time, mass-to-charge ratio pairs, $Rt-m/z$, corresponding to metabolites included in the analysis are fed into the program. Associated extracted ion chromatograms (mass tolerance window = 0.05 Da) are then peak-detected and noise-reduced in both the LC and MS domains such that only true metabolite related features are processed by the software. A list of chromatographic peak areas is then generated for each sample injection. Normalization factors were calculated for each metabolite by dividing their intensities in each sample by the recorded intensity of an appropriate internal standard in that same sample, following the procedure described by (Martínez-Arranz et al., 2015).

Data analysis including peak smoothing and integration of areas under the curves for each ion was performed by Masslynx 4.1 software. The semi-quantitation of individual metabolites was normalized with the respective internal standards, and calculated with the formula as follows. Analyte Conc.($\mu\text{g/ml}$) in Worm Sample = $\text{Area (analyte MRM peak)} \times \text{Standard Conc.}(\mu\text{g/ml}) / \text{Area (Standard MRM peak)}$.

2.12. Multivariate data analysis

Once normalized, the dimensionality of the complex data set was reduced to enable easy.

visualization of any metabolic clustering of the different groups of samples. This was achieved by multivariate data analysis, including the non-supervised principal components analysis (PCA), and supervised orthogonal partial least-squares to latent structures (OPLS-DA) approaches as described previously (Barba et al., 2008). Briefly, in PCA the data matrix is reduced to a series of principal components (PCs), each a linear combination of all metabolite peak areas. Each successive PC explains the maximum amount of variance possible, not accounted for by the previous PCs. OPLS-DA, on the other hand, organizes the dataset variance in order to maximize the difference between groups and minimize intragroup variance. OLPS-DA models were validated using CV-ANOVA (doi: 10.1002/cem.1187). Variables relevant to the discriminant models were selected using S-plots and (Variable importance in the projection) VIP analysis (Lema et al., 2020).

3. Results

3.1. *RAC1/ced-10* mutants exhibit decreased accumulation of Asyn before reaching adulthood in *C. elegans*.

We have previously shown that *RAC1/ced-10* loss of function accelerates Asyn deposition in aged worms, using a nematode model of PD expressing Asyn in muscle (Kim et al., 2018). In this context, our initial focus was on determining if the aggregation of Asyn induced by *RAC1/ced-10* loss-of-function occurs prior to adulthood. This inquiry is crucial for establishing the baseline in the examination of early events associated with PD. Consequently, we explored the impact of *RAC1/CED-10* function during the early stages of development. In *C. elegans* development, there are four larval stages before adulthood, named L1-L4. L1 is the first stage after hatching, and L4 is the phase before development into gravid adults (Fig. 1).

We analyzed the influence of *RAC1/ced-10* mutation in Asyn accumulation at L1 and L4 larval stages because they are the most unequivocally defined stages of development, and both are the most extended periods in fed animals at 20°C (12 h vs 9 h observed at L2 and L3 wild type worms). The effect of *RAC1/CED-10* altered function on Asyn accumulation was investigated in the strain EDC101 harboring the *ced-10(n3246)* mutation in which Asyn is fused to Yellow Fluorescence Protein (YFP) under the control of the muscle-specific *unc-54* promoter, transgene *pkl52386* [*Punc-54::Asyn::YFP*] (Kim et al., 2018) (Sup. Fig. S1). Muscle expression has been used successfully to model protein-misfolding diseases and to identify modifier genes without considering neuronal effects (Van Ham et al., 2008), (Hamamichi et al., 2008). *ced-10(n3246)* mutation is a G-to-A transition resulting in a change of glycine at amino acid position 60 of CED-10 to arginine (G60R) which results in non-null altered function, affecting GTP hydrolysis (Cabello et al., 2014). For simplicity, *ced-10(n3246)* mutants are named *ced-10*, when referring to nematode results obtained for the present manuscript, or *RAC1/ced-10*, all other cases, throughout the manuscript.

RAC1/ced-10 mutant animals at L1 can be distinguished using DIC-Nomarski microscopy by the presence of non-engulfed apoptotic cells in the head in comparison to control animals, without the mutation ((9) and Fig. 2A). Asyn aggregation was not observed at L1 in any of the genotypes. Nevertheless, at L4 the *ced-10* mutation almost doubles the apparent density of Asyn aggregates compared with control animals (42

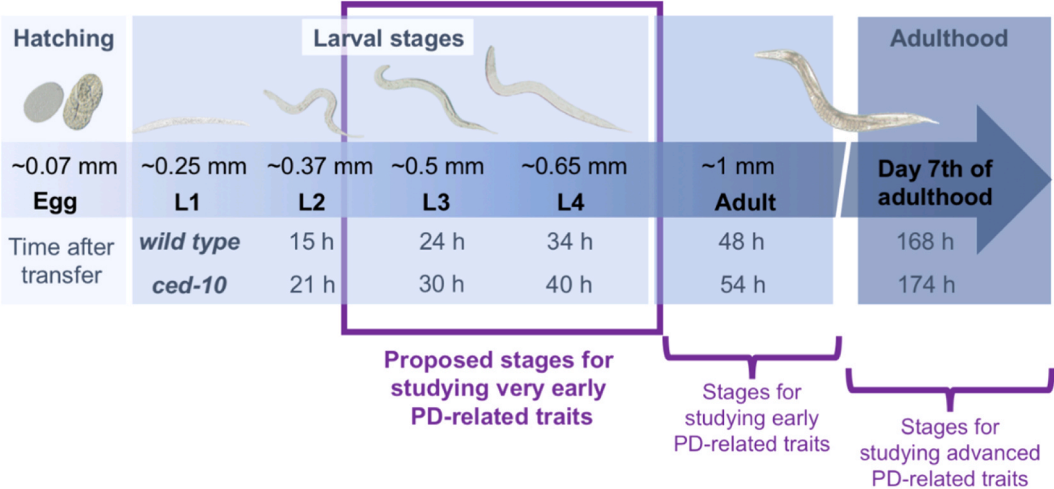


Fig. 1. *RAC1/ced-10* *C. elegans* development cycle. Development stages in worms are divided into four larval stages before arriving at adulthood. Embryo development and hatching occurs in 10 h, and they only develop further once the food is introduced to the system. After adding food, wild-type L1 worms grown at 20 °C will develop to the L2 stage in 15 h, then in 9 h to the L3 stage, and finally in 10 h to the L4 stage, the last before the adult stage is achieved 12 h later. Total lifespan lifespan is about 3 weeks. Usually, PD related symptoms are studied at day 5th or 7th of adulthood. In this article, we propose the interval of larval stages to study early PD-related traits, considering the absence of Asyn in the worm; wt is wild-type and *ced-10* is the nematode *RAC1/ced-10* mutant, genotyped *ced-10(n3246)*.

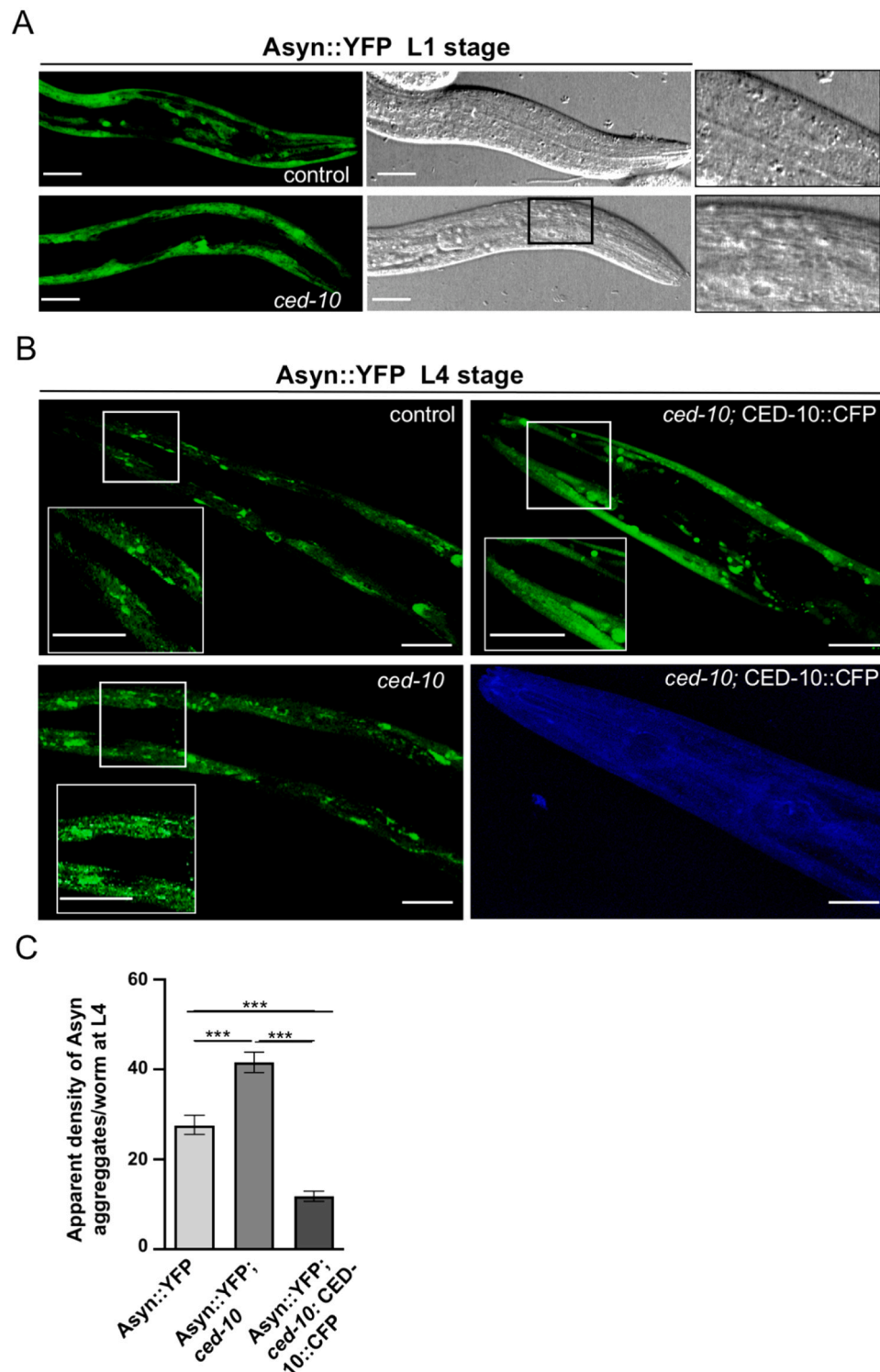


Fig. 2. : Asyn inclusions are observed in *C. elegans* at L4. (A) Confocal fluorescence (left) and DIC (right) images of freshly hatched L1 larvae containing the array *pkIs2386* [*Punc-54*:: Asyn::YFP] expressing Asyn in body wall muscle with and without the *ced-10* mutation. Magnification bar is 20 μ m as indicated. (B) CED-10 decreases Asyn inclusions in *C. elegans*. Representative confocal pictures obtained from animals containing the genomic array *pkIs2386* [*Punc-54*:: Asyn::YFP] expressing Asyn in body wall muscle cells at L4 days of development. Green fluorescence in all figures represents Asyn::YFP inclusions in muscle cells. A representative area was highlighted and expanded in each panel, to better visualize the Asyn::YFP accumulation. (B, first panel, up left) Asyn inclusions were detected in a *C. elegans* model of Asyn misfolding in which Asyn is expressed under the control of the *unc-54* promoter. (B, second panel, bottom left) Asyn apparent aggregates are increased in *ced-10* mutant nematodes. (B, third panel, up right) CFP::CED-10 expression (array *baEx167* [*Pced-10*::CFP::CED-10]) decreased the number of Asyn inclusions in a *ced-10* mutant background. (B, fourth panel, bottom right). The cyan fluorescence marker (CFP) represented the endogenous expression of CED-10 in a *ced-10* background for rescuing Asyn accumulation. Magnification bar is 10 μ m. (C) Quantification of the number of Asyn inclusions per area at L4. Data are mean \pm SEM. Between 30–35 animals were analysed per genotype. Three different transgenic lines expressing CFP::CED-10 were generated and analysed independently. Statistics: One-way ANOVA with a Tukey post hoc test. *** $P \leq 0.005$.

$\pm 9\%$ vs $26 \pm 7\%$, respectively $***P < 0.001$) (Fig. 2B-C). These results indicated a deleterious effect of the *ced-10* mutation in the generation of Asyn aggregates at this larval stage. Importantly, the increase in Asyn

apparent aggregates was abolished in transgenic *ced-10* mutants expressing the CFP::CED-10 fusion protein (Kim et al., 2018) (array *baEx167[Pced-10::CFP::ced-10]*) ($12 \pm 5\%$ in worms expressing CED-10

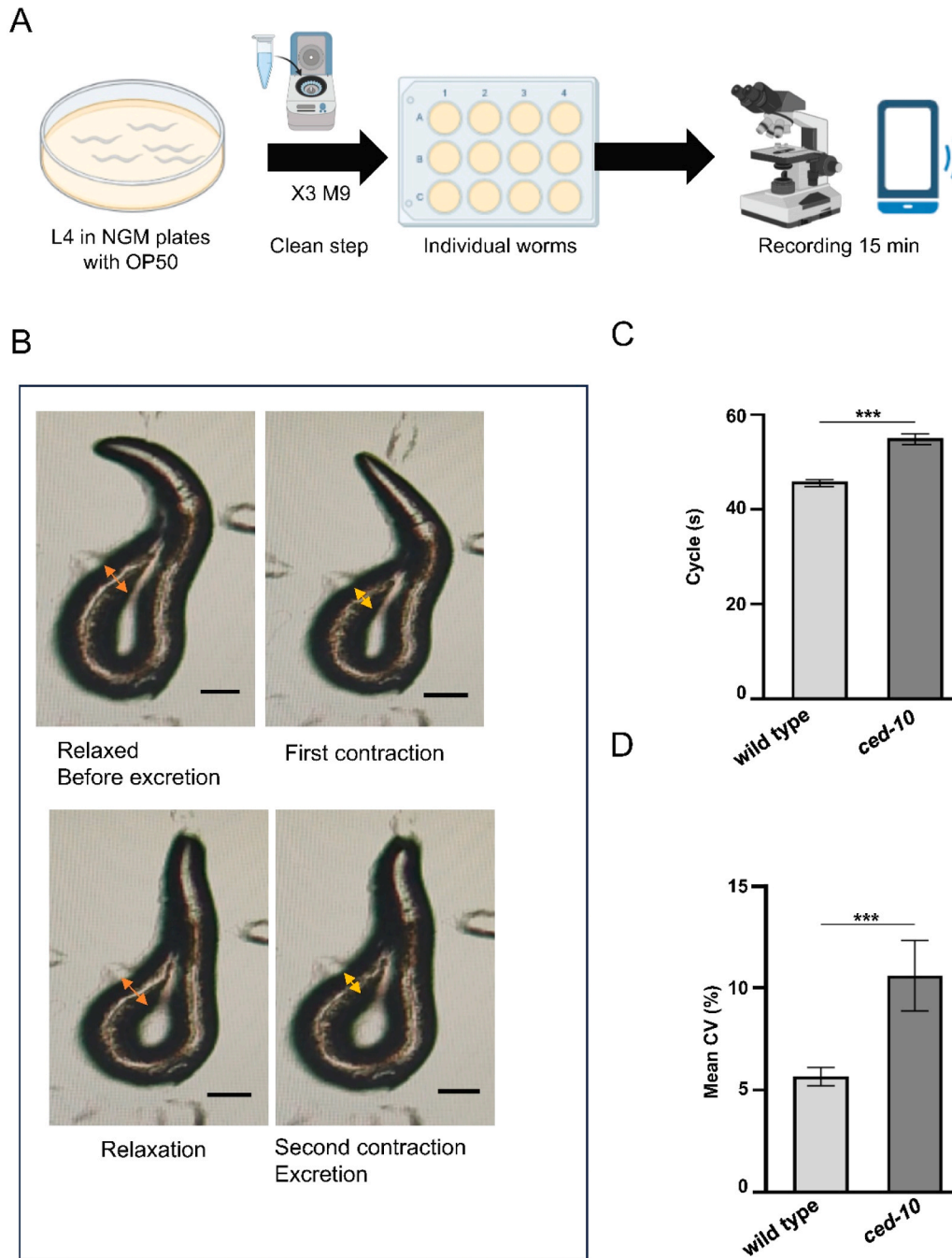


Fig. 3. RAC1/*ced-10* mutant worms display both altered defecation and GABAergic morphology before the adult stage. Part A, (A-B) *C. elegans* defecation cycle studies. A) We performed a protocol based on (Bassan et al., 2010) with slight modifications. Wild type and *ced-10* mutant worms were cultured in NGM plates with OP50 until they reached the L4 stage. Afterward, worms were cleaned with M9 buffer thrice (1 min at 4400 rpm). Worms were individually transferred to 12-well plates with seeded OP50. After 1 h for worms to adapt to the new plate, defecation cycles were recorded for 15 min (~15 cycles). B) *C. elegans* defecation cycle in images. At the beginning of defecation, the digestive tract in the anterior part is relaxed, then is contracted, relaxed, and finally, it employs to expulse the undigested substances. (C-D) *ced-10* mutant worms displayed slow defecation rate compared to wild types. (E) Representative fluorescence images of GFP-labeled GABAergic neurons showing axonal abnormalities at the indicated genotypes. Yellow asterisks indicate axonal abnormalities. All worms are oriented with the anterior end left and ventral side down. Scale bars are 50 μ m and 25 μ m for whole worms and enlarged, respectively; *ced-10* mutation increases the number of axonal abnormalities (bottom panels) in comparison to controls, without the *ced-10* mutation, (upper panels) ($n = 30$ for each phenotype). (F) Quantification of axonal abnormalities. $n = 30$ worms per genotype. Data represent the mean \pm standard deviation (SD). Statistical analysis was carried out with Student's t-test, (* $P < 0.05$; ** $P < 0.01$; *** $P < 0.001$). (G) Thrashing behavior analyzed at L4 ($n = 30$ for each phenotype). Individual worms were located on a microscope slide, containing an agar pad and one drop of M9 buffer. After 2 min of habituation, the movement was analyzed. Data represent the mean \pm standard deviation (SD). Statistical analysis was carried out with Student's t-test, (* $P < 0.05$; ** $P < 0.01$; *** $P < 0.001$).

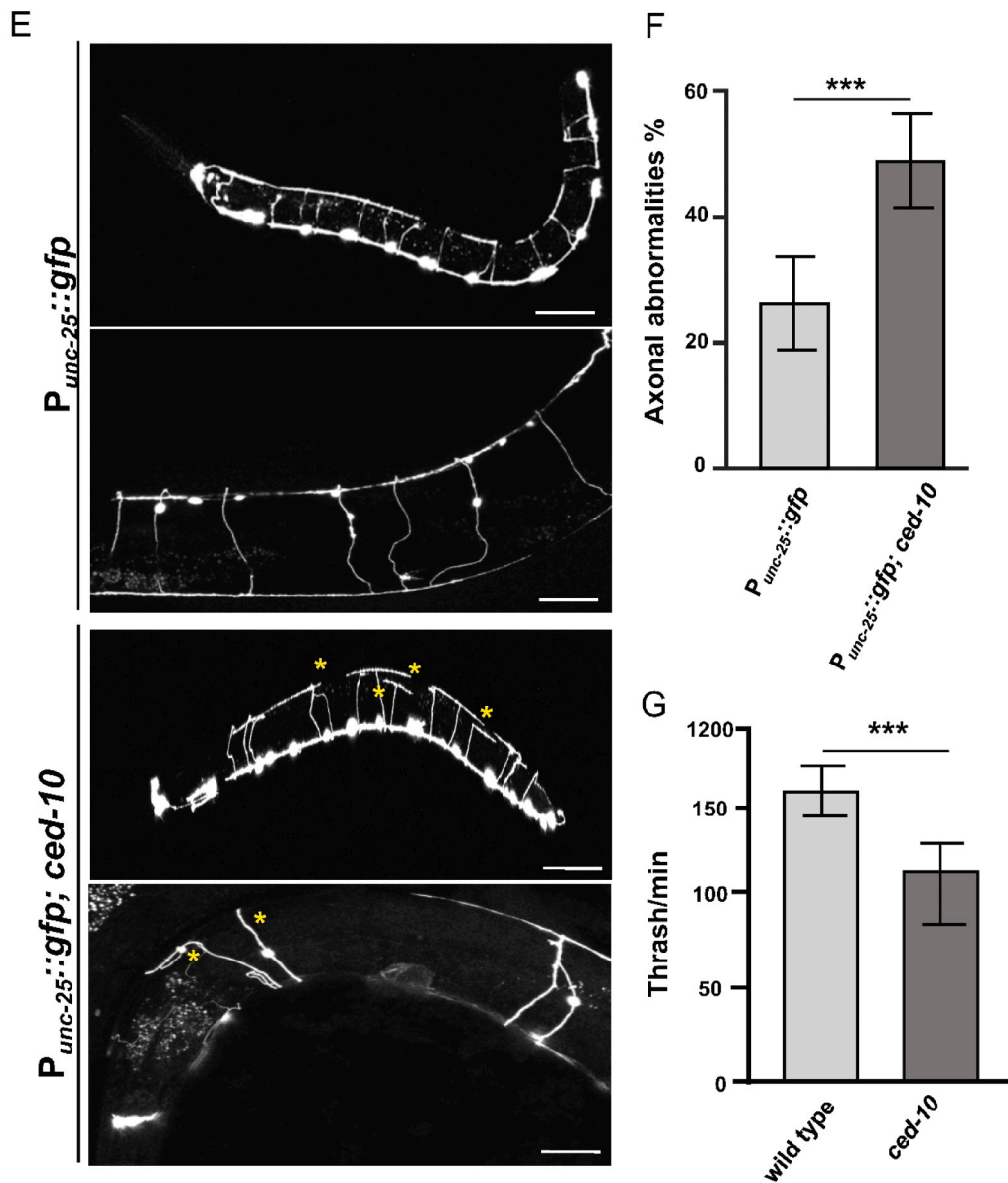


Fig. 3. (continued).

wild type vs. $42 \pm 9\%$ in *rac1/ced-10* mutant worms $***P < 0.001$) (Fig. 2B-C). Then, Asyn accumulation was already influenced by a decrease in the activity of CED-10 at young stages of development.

3.2. *RAC1/ced-10* mutant worms display both altered defecation program and impaired GABAergic morphology before reaching the adult stage

Constipation can be detected as early as two decades before the diagnosis of motor-PD, making it one of the initial recognizable signs indicating the onset of the disease.

Yu et al. (2018). The defecation motor program in *C. elegans* consists of rhythmic cycles regulated by a complex genetic network (BRANICKY and HEKIMI, 2006) in which Rho/rac GTPases take part, and RAC1/CED-10 is among them. Specifically, RAC1/CED-10 is involved in the downstream cascade that keeps the cycle going every 45 s (BRANICKY and HEKIMI, 2006). As such, we evaluated if our *C. elegans* model had the defecation program altered at L4. Following the protocol described in (BRANICKY and HEKIMI, 2006) and summarized in Fig. 3 (Fig. 3, A-B), wild-type and *ced-10* worms, both at L4, were transferred

to 12 well-plates with an overnight OP50 lawn and individually recorded for 15 cycles (~15 min).

As illustrated in Fig. 3C, *ced-10* mutant animals had longer defecation cycles (55 ± 12 s) than wild type worms (45 ± 5 s, $***P < 0.001$) (Fig. 3C). The defecation cycle in *C. elegans* is characterized by its regularity (BRANICKY and HEKIMI, 2006). Consequently, we measured the cycle variation by calculating the mean coefficient of variation (CV), which correlates with cycle regularity (BRANICKY and HEKIMI, 2006). We observed that *ced-10* mutants had almost doubled the mean CV in comparison with wild-type worms ($11 \pm 6\%$ vs $6 \pm 2\%$ $*P < 0.05$). Altogether these results indicated that the defecation cycle was longer and more irregular in *ced-10* mutants compared with wild type worms at L4.

Defecation cycles in *C. elegans* require the coordination of specific muscles, a couple of neurons, and the neurotransmitter GABA (BRANICKY and HEKIMI, 2006). Indeed, the defecation behavior depends on the integrity of GABAergic neurons (McIntire et al., 1993). As GABA regulates the defecation program in mammals and in *C. elegans* (Mahoney et al., 2008; Murueta-Goyena et al., 2019), and considering that GABA signaling is altered in PD (Murueta-Goyena et al., 2019), we

examined the GABAergic morphology using our *RAC1/ced-10* mutant nematodes. GABAergic cell bodies and axons in *C. elegans* can be visualized using the reporter strain CZ1200 *juIs76* [*Punc-25::GFP*] to investigate neurodegeneration in the nematode (Coppa et al., 2020). The *unc-25* gene encodes the human glutamic acid decarboxylase (GAD) orthologous gene, glutamate decarboxylase 1. In worms expressing this reporter, the GFP fluorescence is observed along the ventral cord axons

and in the GABAergic cell bodies (Coppa et al., 2020). To explore the influence of *ced-10*, first on GABAergic morphology, *juIs76* [*Punc-25::GFP*] animals were crossed with *ced-10* (*n3246*) mutant worms, strain EDC073 (see methods and Sup. Fig S1) and the percentage of axonal defects in the resulting progeny was quantified, as described in (Coppa et al., 2020). Neuronal deficits were barely observed in wild-type worms without the mutation ($27 \pm 7\%$) (Fig. 3E and F). In contrast, the *ced-10*

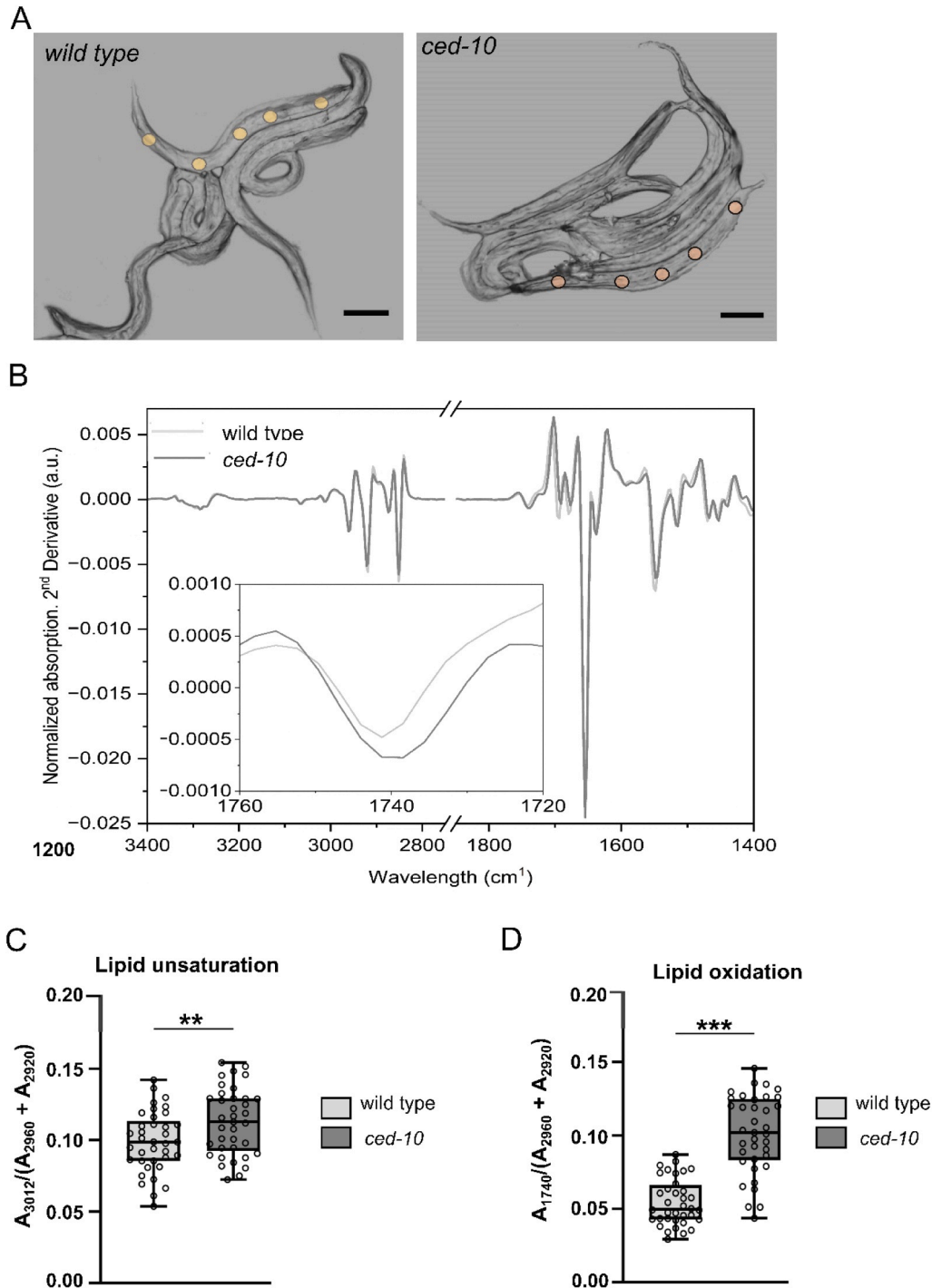


Fig. 4. *RAC1/ced-10* mutant worms analyzed by SR-μFTIR displayed increased lipid unsaturation and peroxidative damage (A) *C. elegans* wild type and *ced-10* dried over CaF2 for SR-μFTIR measurements at L3 stage of development. FT-IR spectra were obtained for 10 worms at 5–6 different locations along the worm. As an example, some yellow points are drawn along the worms. Scale bar= 30 μm. (B) 2nd derivative of the mean SR-μFTIR spectra of wild type (gray) and *RAC1/ced10* (black) L3 worms. The inset shows the amplification of the carbonyl group at 1740 cm⁻¹. (C) Lipid unsaturation ratio (C=C / (CH2 +CH3) $A_{3012} / A(2920 + 2960)$) of all spectra acquired for wild type and *ced-10*. *** $p < 0.001$ In box plots, the bars indicate the maximum and minimum values, the horizontal line represents the average and each point represents one spectrum. (D) Lipid oxidation ratio (COOH/(CH2 +CH3)) ($A_{1740} / A(2920 + 2960)$) of all spectra, for both strains.

mutation increased almost twice the GABAergic damage at L4 ($49 \pm 8\%$, $***P < 0001$) (Fig. 3E, F). The loss or injury of GABAergic neurons alters locomotion (McIntire et al., 1993). The motility was evaluated by the thrashing assay, in which nematodes were placed in liquid, and the frequency of lateral swimming or thrashing movements was estimated (see methods). Thrashing was reduced in *ced-10* mutant animals compared to wild-type (Fig. 3G) 156 ± 15 thrashes per minute in controls vs 114 ± 15 in worms containing the mutation, $***P < 0001$. Thus, altered RAC-1/CED-10 activity disrupted the defecation cycle, and led to aberrant GABAergic axonal morphology and function.

3.3. Increased lipid unsaturation and peroxidation characterize young *RAC1/ced-10* worms

Altered unsaturated lipids underlie brain synucleinopathies, including PD (Fu et al., 2022). In particular, plasma polyunsaturated fatty acid levels are aberrant at the early stages of the disease, independently of food intake (Yoo et al., 2021). To evaluate lipid unsaturation in *C. elegans*, we used synchrotron Fourier-Transform Infrared spectroscopy (sFT-IR). Infrared spectra were collected at different locations of *ced-10* mutant and wild-type nematodes at L3 (yellow dots in Fig. 4A), because L4 worms were too thick to be analysed by sFT-IR (16).

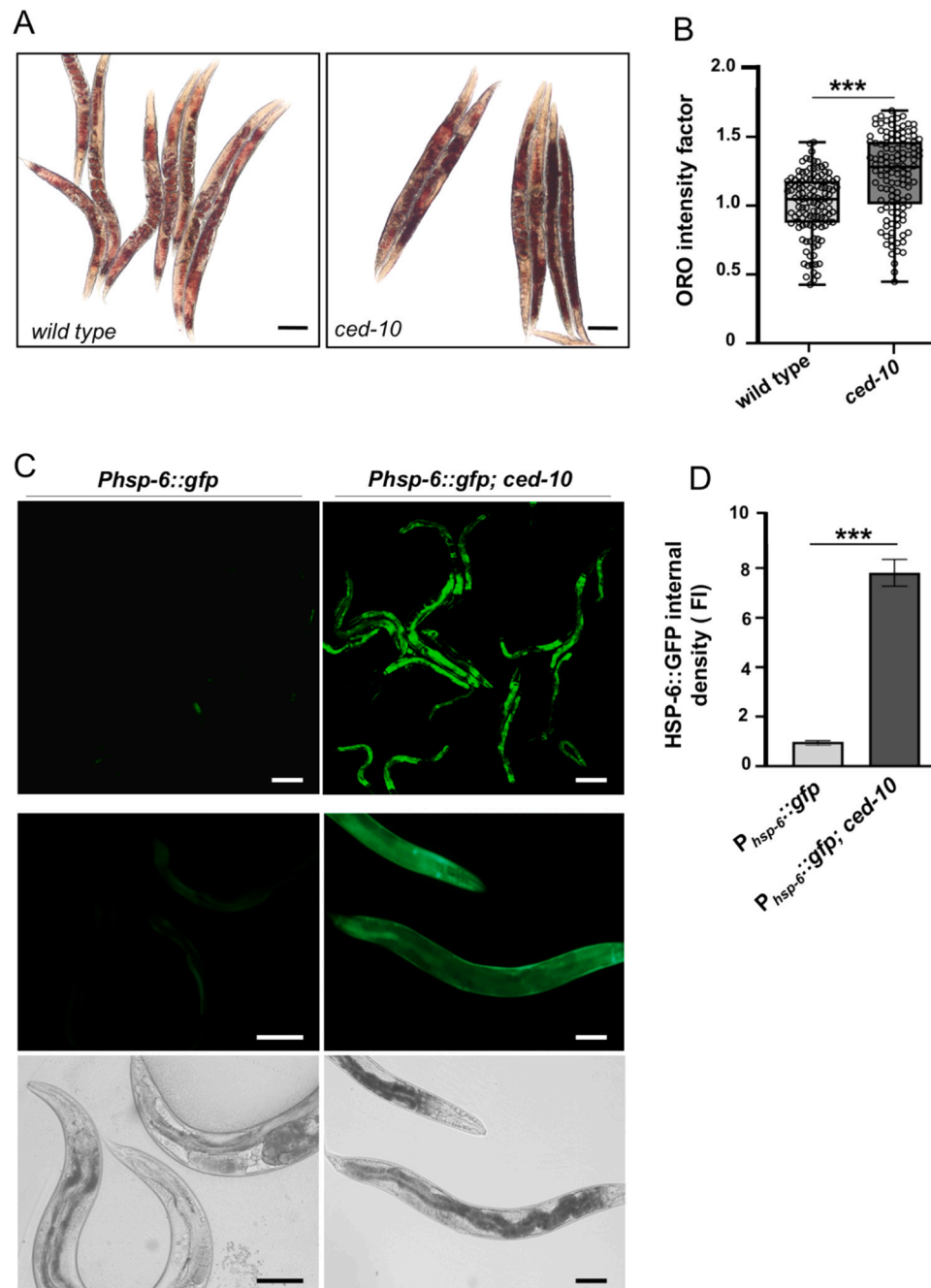


Fig. 5. *RAC1/ced-10* mutant worms display lipid accumulation. (A) ORO staining of wild type and *ced-10* L4 animals. Images were taken using the same light exposure. Scale bar is 50 μ m (B) ORO intensity factor, relative to wild type and *ced-10* worms. $n = 120$ and $N = 3$. (C) Mitochondrial stress response without and with the *RAC1/ced-10* mutation (left and right panels respectively). Scale bar is 100 μ m. Mid panels and bottom panels correspond to higher magnification images to better visualize the fluorescence with the corresponding bright field photomicrographs. Scale bar is 40 μ m. (D) Quantification (fold increase) of the mitochondrial stress response indicated as GFP internal intensity. 30 worms were used, and the experiment was repeated three times.

The absorption bands assigned to the lipid groups were analyzed using the second derivative of the spectra to avoid baseline contribution and to ensure a better resolution of the maximum of each band. The second derivative of the averaged spectra for both conditions is shown in Fig. 4B.

To study lipid unsaturation levels, we focused on the analysis of the carbon double bonds (C=C) in the infrared (IR) absorption spectrum, which absorb at 3012 cm^{-1} (Benseny-Cases et al., 2014). Lipid unsaturation levels were computed by normalizing the absorption of unsaturated C=C bonds by the total lipid content (sum of the absorption of chemical groups C-H of CH_2 and C-H of CH_3 , with band absorptions at 2920 cm^{-1} and 2960 cm^{-1} , respectively (17)) to avoid the influence of sample thickness. As shown in Fig. 4C, *ced-10* mutant worms displayed increased levels of unsaturated bonds compared with the wild-type animals at the same stage (Fig. 4C). The abundance of unsaturated lipids increases susceptibility to lipid peroxidation, a process of oxidative degradation of cellular lipids that contributes to the pathogenesis of neurodegenerative diseases (5). Since lipid carbonyls could be formed as consequence of lipid oxidation from unsaturated lipids (14), we hypothesized that an increase in unsaturated lipids could be translated as an increase in lipid peroxidation. Carbonyl groups (-CHO) could be formed as a oxidation product of the carbonate chain resulting in the formation of carbonyl groups in the carbonate chain or as oxidation products such as 4-hydroxynonenal. This carbonyl groups have a clear band at 1740 cm^{-1} in the IR spectrum (17). The inset in the second derivative of the average spectrum of each condition (Fig. 4B) shows a higher intensity of the band-specific of carbonyls at 1740 cm^{-1} in *ced-10* mutants than in wild-type worms. The ratio of carbonyl bands was normalized to total lipid content. Fig. 4D shows increased lipoxidative damage in *RAC1/ced-10* mutants compared with wild-type worms ($p < 0.001$) (Fig. 4D).

3.4. *RAC1/ced-10* mutant animals display lipidomic abnormalities before adulthood

One of the consequences of lipoxidative damage is the formation of lipid droplets (LD) (reviewed in (Islimy et al., 2022)). We investigated the presence of LD in *ced-10* mutants compared to wild type worms at the L4 stage + 1 day of development. Animals were grown at 20°C and stained with Oil Red O (ORO) to quantify overall neutral lipid content in the intestine and the hypodermis (O'Rourke et al., 2009). *ced-10* mutant worms showed increased ORO staining in comparison with wild type (Figs. 5A and 5B).

Fat accumulation leads to mitochondrial damage (21). Similarly, mitochondrial dysfunction contributes to the formation of LD (Lee et al., 2013). Dysfunction of mitochondrial homeostasis induces the *mitochondrial unfolded protein response* (UPRmt), which alters cellular

metabolism. HSP-6 in *C. elegans* is a homolog of the human mitochondrial-specific *heat shock protein 70*, HSP-70, and has been established as an indicator of the UPRmt (Nargund et al., 2012; Yoneda et al., 2004). *ced-10* animals were crossed with the reporter strain *Phsp-6::GFP* and we monitored the UPRmt elicited by the *RAC1/ced-10* mutation. As shown in Fig. 5C, the UPRmt is induced in the mutants and not in the wild-type worms (Fig. 5C). RNAi knockdown of *RAC1/ced-10* activated *Phsp-6::GFP* expression and also, although less significantly, the expression of *Phsp-4::GFP* (Sup. Fig. S2). These results confirmed that a reduction in the expression levels of *RAC1/CED-10* contributed to the triggering of the UPRmt (by the activation of *Phsp-6::GFP*) and the ER stress response, as indicated by the reporter strain *Phsp-4::GFP* (Hou et al., 2014).

To ascertain the specific lipid species accumulated in young mutant worms, we performed a lipidomic analysis at L4. To this end, we compared the non-targeted UPLC-HRMS lipidomic profiles from whole homogenates of wild-type and *ced-10* mutant nematodes. Raw data from the lipidomic analysis showed a general increase in lipid species compared with wild-type (Fig. 6A). This was in agreement with the LD accumulation observed in *ced-10* mutants (Fig. 5A-B). To unbiased the effect of the total lipid content, we normalized the results by dividing the raw data by the sum of the lipid content in each genotype (Fig. 6B).

The principal component analysis (PCA), an unsupervised and unbiased approach, showed a tendency towards clustering between the *rac1/ced-10(green)* and wild type (red) nematodes (Sup. Fig. S3A). The first two components (PC1 and PC2) accounted for 28,8 and 13,6% of the variation respectively. This clustering was confirmed by a discriminant model (Sup Fig. S3B) OPLS-DA ($Q^2 = 0.645$; $p = 0.01$) further supporting the fact that mutant worms have different metabolic network than wild type ones. A general heat map comparing both genotypes showed a general increase (intense red color in Fig. 7A) in different lipid metabolites, including some triacylglycerides (TAG), phosphatidylcholines (PC) and sphingomyelins (SM) (Fig. 7A). Only PC and SM are significantly altered as indicated by the gray line. A detailed heat map of PC and SM species revealed that those with significant changes were PC (O-18:0/18:2) and SM (31:1) (Fig. 7B). Altogether, *RAC1/ced-10* nematodes could serve as a promising tool to determine specific lipid alterations often attributed to early PD.

4. Discussion

Here, we present *RAC1/ced-10* mutant nematodes as a promising model for investigating early stage, focusing on non-motor symptomatology. These mutants mimic constipation (by an impairment in the defecation cycle) and GABAergic abnormalities before adulthood. In addition, these nematodes show impaired lipid metabolism compared with wild-types. In particular, *RAC1/ced-10* worms exhibit increased

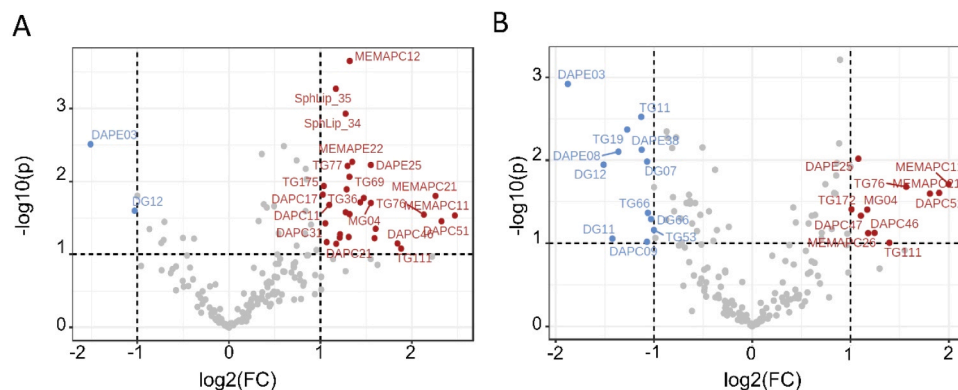


Fig. 6. : Analysis of the lipid profiling. Volcano plots of the raw data (A) shows an increase in many lipid metabolites in *ced10* mutants consistent with the increase in total lipid composition. When data are normalized for the total lipid amount, the resulting volcano plot (B) shows increased and decreased metabolites between wild-type and control worms.

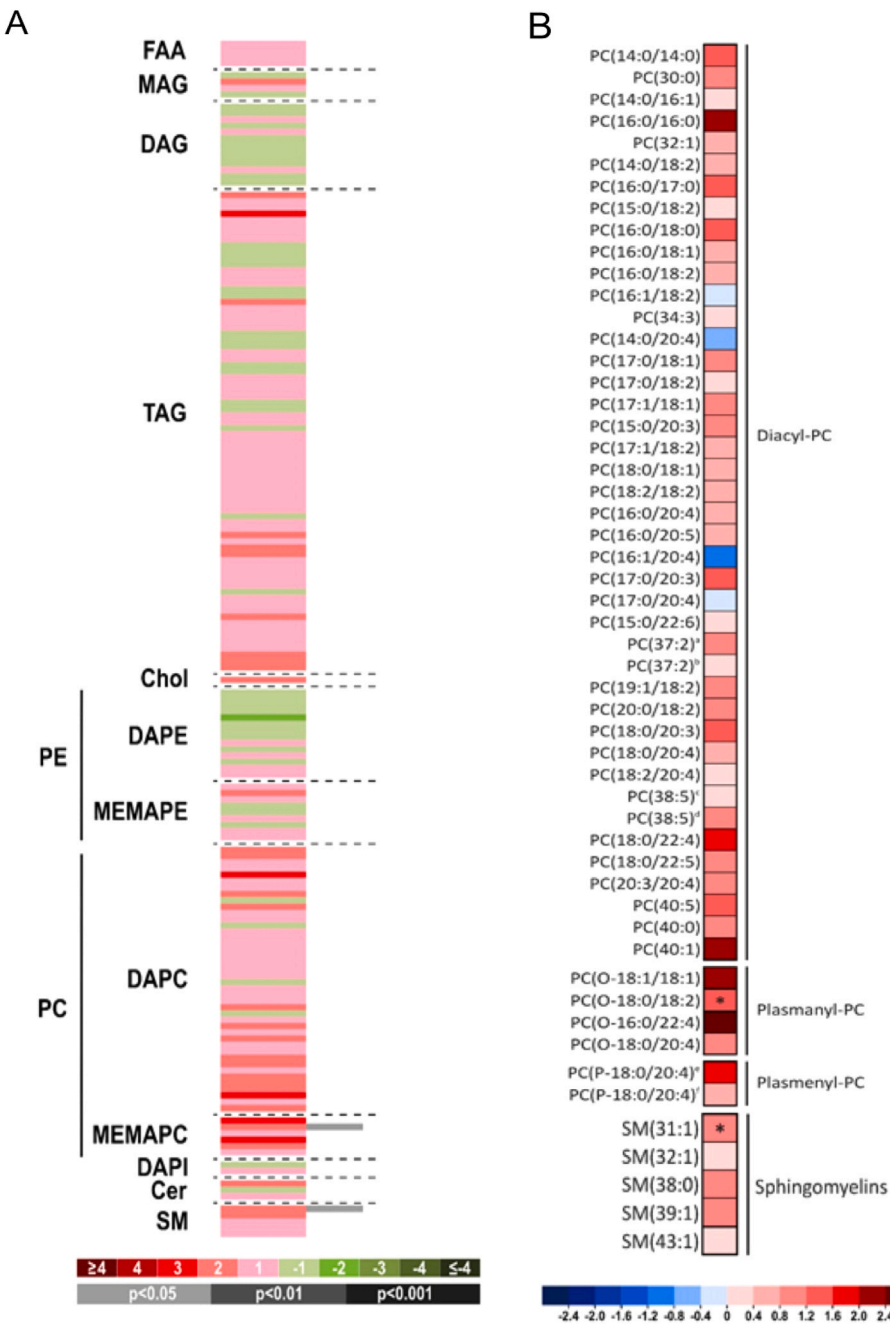


Fig. 7. *RAC1/ced-10* nematodes display an altered lipidomic fingerprint. A) General heat map showing lipid species ordered according to their carbon number and the acyl chain degree of unsaturation. For each comparison, log transformed ion abundance ratios are depicted, as represented by the scale. The heat map color scale denotes to the relative content of lipid species in *ced-10* mutant vs wild-type nematodes. Dark red indicates the highest increases, dark green indicates the most pronounced decreases. Gray lines correspond to significant fold-changes of individual metabolite levels, darker gray colors have been used to stress higher significance. ($P \leq 0.05$, Student's t-test). B) Specific heat map showing PC and SM species ordered according to their carbon number and the acyl chain unsaturation degree. For each comparison, log transformed ion abundance ratios are depicted, as represented by the scale. The heat map color scale denotes to the relative content of lipid species in *ced-10* mutant vs wild type. Dark red indicates the highest increases, dark blue indicates the most pronounced decreases. Asterisks correspond to the significant fold-change of individual metabolite levels ($P \leq 0.05$, corrected for multiple comparisons).

unsaturation and lipoxidation indices, together with an increase in lipid droplet content. Lipidomic fingerprinting reveals that PC and SM are the most significantly increased lipid species.

ced-10 mutant worms show a decrease in dopaminergic function and an increase in autophagic vesicles. Through experiments using these worms, it was revealed that CED-10 has a protective role in dopaminergic neurons within transgenic nematodes that overexpress human Asyn, mitigating Asyn-induced toxicity. Moreover, the expression of RAC1 in PD-derived dopaminergic neurons rescues Asyn accumulation,

cell death, and autophagy impairment (Kim et al., 2018). This suggests a cell-autonomous mechanism wherein *RAC1/ced-10* activity impacts dopaminergic neurons. However, considering the cell non-autonomous mechanisms implicated in PD pathogenesis (Panicker et al., 2021), the possibility of a non-cell-autonomous action of *RAC1/ced-10* loss-of-function cannot be dismissed. Several PARK proteins, such as PARKIN and LRRK2, known to contribute to non-cell-autonomous mechanisms of neuron death, interact with RAC1 (Cabello et al., 2014) and (Chan et al., 2011) respectively). PARKIN, which functions as

an E3 ligase, regulates RAC1 expression (Cabello et al., 2014) while the interaction between LRRK2 and Rac1 modulates neurite retraction (Chan et al., 2011). Since these PD-associated proteins are expressed in various cell types within or outside the central nervous system, they may amplify harmful signaling. As such, it is tempting to speculate that RAC1/*ced-10* could potentially modulate non-cell-autonomous processes associated with PD, through interactions with these (or other yet unidentified) proteins expressed in diverse cell types (Hinkle et al., 2019) and (Kam et al., 2020).

Asyn accumulation is one of the main hallmarks of PD, and it parallels neurodegeneration. Nevertheless, whether Asyn seeding is a cause or consequence of neurodegeneration remains controversial. The existence of an animal model to study the timepoint at which Asyn starts to accumulate, may help to investigate the initiation and progression of PD. *C. elegans* models have been developed to investigate the mechanisms of Asyn aggregation (Van Ham et al., 2008; Hamamichi et al., 2008; Kim et al., 2018) and have been widely and successfully employed for the investigation of late PD. Unfortunately, none of these has been used to investigate the changes linked to earlier stages. These stages cover a long latent phase of PD and, as such, represents an opportunity for early recognition of incipient PD. Because strain EDC101 (Sup. Fig. S1) has human Asyn expression and harbors the *ced-10* mutation (Kim et al., 2018), we can delineate several traits that are independent of Asyn accumulation. This has two main advantages. First, it allows for the study of early events linked to Asyn aggregation induced by RAC1/*ced-10* altered function. Second, it also enables exploration of early phenomena linked to PD. We established L4 as the first larval stage in which we observe incipient accumulation of Asyn without affecting regular movement (data not shown). In addition, the dopaminergic function is also altered in RAC1/*ced-10* mutants at L4 (Kim et al., 2018). Together with the lipoxidative alterations observed, this marks the L3 to L4 + 1 day interval of development as the most suitable larval stage for investigating early stages of PD in *C. elegans*.

PD is a multi-systemic disorder with a heterogeneous early phases showing a broad range of non-motor symptoms (Schapira et al., 2017). Constipation is among the first incipient manifestations, occurring up to 20 years prior to the first motor symptoms (Yu et al., 2018). In addition, early constipation predicts faster onset of dementia in PD (Camacho et al., 2021). RAC1 variants that affect GTP hydrolysis have been associated with constipation in some neurodevelopmental disorders in humans (Banka et al., 2022). The *ced-10*(n3246) mutation characterizing our model results in a non-null altered function that affects GTP hydrolysis (Kim et al., 2018). We showed here that RAC1/*ced-10* mutants displayed an altered defecation motor program, namely shortened cycles and slow defecation rates. This agrees with the role of RAC1 in defecation, described in other animal models (Martínez-Sánchez et al., 2023; Barbosa et al., 2020). The defecation motor program in *C. elegans* is regulated by GABAergic signaling. Indeed, the GABAergic neuron AVL participates in controlling the simultaneous contraction of dorsal and ventral anterior body-wall muscles (aBoc) once anterior calcium levels return to baseline (Mahoney et al., 2008). In addition, neuropeptides released from the intestine depolarize the GABAergic DVB motoneuron, which, in turn, stimulates the contraction of the enteric muscle to produce expulsion (Mahoney et al., 2008). We showed that RAC1/*ced-10* mutants displayed altered GABAergic neurons and axons at the L4 stage. Therefore, we are tempted to speculate that the impairment in the defecation motor program observed in the nematode might be a consequence of altered GABAergic neurons and their projections. In this sense, impairment of intestinal motility in PD is partially due to dysregulation of GABAergic signaling (Auteri et al., 2015). Therefore, we are confident that RAC1/*ced-10* mutants might be a useful tool to investigate other PD symptoms in which GABA signaling is altered.

Considering the role of dysregulated GABA signaling in seizure disorders, it is significant that a recent clinical report on early PD etiology, people with epilepsy have a 2.5 times greater chance of developing PD in their lifetimes than those in the general population (Simonet et al.,

2022). Conversely, people diagnosed with PD are at greater risk of experiencing seizures (Gruntz et al., 2018). Interestingly, we previously reported that a *ced-10* (n3246) gain-of-function allele that displays axon-pathfinding defects similar to those resulting from multiple Rac loss-of-function mutations, led to increased susceptibility to an GABA-dependent epileptic-like convulsion behavior in *C. elegans* (Locke et al., 2009). Given the function of RAC1 in modulating cytoskeletal dynamics, including synaptic vesicle trafficking, polymorphisms in this and related genes might represent a source of aberrant neuronal hyperexcitation with a contribution to early events in PD. An increased application of *C. elegans* to accelerate functional annotation of human genomic variations of unknown significance might prove useful in this scenario (Mew et al., 2022).

Growing evidence demonstrates that PD shows lipid alterations and, hence, is also considered a “lipidopathy” (Fanning et al., 2020). However, it is unclear whether the misfolding of Asyn precludes lipid alterations. Thus, it is controversial whether PD is a protein-induced lipidopathy or a lipid-induced proteinopathy. Recent advances point to the first option, because the main neurotoxic process is an imbalance in cellular lipid metabolism, in which Asyn dyshomeostasis is the trigger (Fanning et al., 2020). *C. elegans* does not have a homolog of Asyn. As such, the PD-like phenotypes in young RAC1/*ced-10* mutants shown here, appeared without the influence of Asyn. Therefore, this organism provides us the opportunity to identify potential synergisms between Asyn and lipid metabolism at early stages when Asyn starts to accumulate.

In the present work, we demonstrated that RAC1/*ced-10* mutants displayed an increased unsaturation index, suggesting an increase in the content of polyunsaturated fatty acid (PUFA), and lipoxidative damage. Recently, it has been described that, in human PD, some unsaturated fatty acids are specifically elevated in the amygdala, where Asyn is commonly accumulated, correlating with an increase in lipoperoxidation (Fu et al., 2022). Interestingly, in the cerebral cortex of asymptomatic patients at early stages of parkinsonian neuropathology, where Asyn deposits are not yet observed, both lipoxidative damage and PUFA ω -3 content are elevated (Dalfó and Ferrer, 2008). As such, RAC1/*ced-10* mutants, in which Asyn is absent, recapitulate several lipidomic traits observed at early timepoints PD.

Phosphatidylcholine (PC), phosphatidylethanolamine, phosphatidylserine, and sphingomyelin (SM) are unsaturated fatty acids that are increased in the amygdala of late PD patients (Fu et al., 2022). Among these, PC and SM, but not phosphatidylethanolamine or phosphatidylserine, were elevated in the RAC1/*ced-10* mutant nematodes. The specific increase in these two lipid species prompted us to speculate that they may be altered at the beginning of PD. SM accumulation could be also a consequence from an increase in PC levels. SM is synthesized by SM-synthase using both PC, as donor of a phosphorylcholine group, and free ceramide. Accordingly, the elevated PC content as main cause for the higher levels of SM observed in RAC1/*ced-10* mutant worms is the most plausible explanation.

PC and SM are in the core of Lewy bodies observed in postmortem samples of PD patients (den Hartog Jager, 1969). It is worth mentioning that Lewy bodies are already present in brain areas of asymptomatic PD, indicating that PC and SM metabolism could be impaired before neurodegeneration appears. In addition, both PC and SM are implicated in PD pathogenesis favoring Asyn aggregation. In this sense, PC modifies the secondary structure of Asyn oligomers formed in vitro at the early stages of protein aggregation (den Hartog Jager, 1969). In the case of SM, the relationship is more indirect. The lack of glucocerebrosidase 1 and the resultant increase in ceramides and SM, promotes the formation of abnormal oligomers of Asyn. In turn, elevated levels of Asyn species result in reduced glucocerebrosidase 1 activity, which further stabilizes Asyn oligomers (Nuzhnyi et al., 2015). Asyn-lipid binding, and its subsequent oligomerization, is dependent on the composition of membrane phospholipids with preferential binding to regions enriched in sphingolipids, such SM (Makasewicz et al., 2021). Considering that *C. elegans*

does not express Asyn, but *RAC1/ced-10* mutation increases Asyn aggregates in the Asyn-expressing strain *Punc-54::Asyn* at L4, we are tempted to speculate that PC and SM contribute to Asyn seeding at early stages of the disease.

PC and SM are not the only lipid species augmented in the *RAC1/ced-10* lipidome, but a general increase in the lipid content is detected as revealed by the lipidomic profile and the LD quantification. LD are major players in PD progression because of their relevance in neuronal activity (Islimy et al., 2022). Here, we show that the *ced-10* mutation led to an increase in the LD content, which could be a consequence of mitochondrial dysfunction. In this sense, *RAC1/ced-10* mutants display a higher ratio of mtDNA mutations (Flowers et al., 2023). Then, we are tempted to speculate that mutations in mtDNA should lead to mitochondrial ROS, impairing mitochondrial metabolism pathways such as lipid beta-oxidation. Interestingly, mtDNA mutations are considered an important factor responsible for the development of mitochondrial dysfunction and neurodegeneration in PD (reviewed in (Buneeva et al., 2020)). Moreover, this is supported by our finding that the UPRmt is strongly upregulated in *RAC1/ced-10* animals. These results, reinforce the utility of *RAC1/ced-10 C. elegans* mutants as a valuable model to go deeply into the physiopathology of PD.

5. Conclusions

The alterations described in *RAC1/ced-10* young nematodes recapitulate some disturbances observed at asymptomatic stages of PD. Concretely, these worms show slow intestinal cycles, decreased defecation rate, GABAergic neuronal damage and alteration in the lipidome. Then, *RAC1/ced-10C. elegans* mutants emerge as an easy-to-manipulate and suitable animal model to go deeply into the knowledge of asymptomatic PD, helping to better manage PD patients and delay neurodegeneration. Therefore, it is tempting to conclude that this nematode model could serve as a tool for establishing a timeline of traits that represent predictive signals of PD, which will contribute to the evaluation of novel therapies and drugs to ameliorate symptoms of PD.

CRediT authorship contribution statement

A. Muñoz: Formal analysis, Investigation, Methodology, Validation, Visualization. **N. Benseny-Cases:** Investigation, Methodology, Validation. **S. Guha:** Investigation, Methodology, Validation. **I. Barba:** Investigation, Methodology. **K.A. Caldwell:** Resources, Validation, Visualization, Writing – original draft. **G.A. Caldwell:** Resources, Validation, Visualization, Writing – original draft. **L. Agulló:** Data curation, Formal analysis, Methodology, Validation, Visualization. **A. Laromaine:** Funding acquisition, Resources, Supervision, Validation, Visualization. **V.J. Yuste:** Data curation, Formal analysis, Writing – original draft, Writing – review & editing. **E. Dalfó:** Conceptualization, Data curation, Formal analysis, Funding acquisition, Investigation, Methodology, Project administration, Resources, Supervision, Validation, Visualization, Writing – original draft, Writing – review & editing.

Funding sources

This work was supported the following grants: Esther Dalfó was supported by the grant PH613883 from the Instituto Carlos III. Esther Dalfó is members of the GENIE and EU-ROS Cost Action of the European Union. This research was supported by the Spanish Ministry of Science and Innovation through the RTI2018–096273-B-I00 and PID2021–122645OB-I00 projects, the 'Severo Ochoa' Programme for Center of Excellence in R&D (CEX2019–000917), the Generalitat de Catalunya (2017SGR765 grant). Amanda Muñoz acknowledges the Ph.D. scholarship (FPU18/05190) in the framework of the Biotechnology Ph.D. program of the UAB.

Declaration of Competing Interest

The authors declare that they have no known competing financial interests or personal relationships that could have appeared to influence the work reported in this paper.

Data availability

Data will be made available on request.

Acknowledgements

We thank Cristina Alonso, from OWL metabolomics (<https://owl-metabolomics.com>) for technical assistance. The genetic strain BR3579 was kindly provided by Dr Ralf Baumeister (Albert-Ludwing University, Freiburg/Breisgau, Germany). The construct *Pced-10::CFP::CED-10* was a generous gift provided by Erik Lundquist (University of Kansas, Lawrence, KS, USA). SR-IFTIR experiments were performed at MIRAS beamline at ALBA Synchrotron with the collaboration of ALBA staff. Figs. 1, 3 and Supplementary Fig. S1 were created using Biorender.com. Amanda Muñoz and Anna Laromaine. participate in the Spanish National Research Council (CSIC) interdisciplinary platform for sustainable plastics toward a circular economy (SusPlast) and in the Aerogels COST ACTION (CA 18125), EPNOE network, Conexión Nanomedicina del CSIC, and Red Nanocare 2.0.

Appendix A. Supporting information

Supplementary data associated with this article can be found in the online version at [doi:10.1016/j.pneurobio.2024.102572](https://doi.org/10.1016/j.pneurobio.2024.102572).

References

- Auteri, M., Zizzo, M., Serio, R., 2015. The GABAergic system and the gastrointestinal physiopathology. *Curr. Pharm. Des.* vol. 21 (34), 4996–5016. <https://doi.org/10.2174/1381612821666150914121518>.
- Banka, S., et al., 2022. Activating *RAC1* variants in the switch II region cause a developmental syndrome and alter neuronal morphology. *Brain* vol. 145 (12), 4232–4245. <https://doi.org/10.1093/brain/awac049>.
- Barba, I., et al., 2008. Nuclear magnetic resonance-based metabolomics predicts exercise-induced ischemia in patients with suspected coronary artery disease. *Magn. Reson. Med* vol. 60 (1), 27–32. <https://doi.org/10.1002/mrm.21632>.
- Barbosa, S., et al., 2020. Opposite modulation of *RAC1* by mutations in trio is associated with distinct, domain-specific neurodevelopmental disorders. *Am. J. Hum. Genet.* vol. 106 (3), 338–355. <https://doi.org/10.1016/j.ajhg.2020.01.018>.
- Bassan, P., et al., 2010. RMieS-EMSC correction for infrared spectra of biological cells: extension using full Mie theory and GPU computing. *J. Biophotonics* vol. 3 (8–9), 609–620. <https://doi.org/10.1002/jbio.201000036>.
- Benseny-Cases, N., Klementieva, O., Cotte, M., Ferrer, I., Cladera, J., 2014. Microspectroscopy (μFTIR) reveals co-localization of lipid oxidation and Amyloid plaques in human Alzheimer disease brains. *Anal. Chem.* vol. 86 (24), 12047–12054. <https://doi.org/10.1021/ac502667b>.
- BRANICKY, R., HEKIMI, S., 2006. What Keeps *C. elegans* regular: the genetics of defecation. *Trends Genet.* vol. 22 (10), 571–579. <https://doi.org/10.1016/j.tig.2006.08.006>.
- Brenner, S., 1974. The genetics of *Caenorhabditis elegans*. *Genetics* vol. 77 (1), 71–94. <https://doi.org/10.1093/genetics/77.1.71>.
- Buneeva, O., Fedchenko, V., Kopylov, A., Medvedev, A., 2020. Mitochondrial dysfunction in Parkinson's disease: focus on mitochondrial DNA. *Biomedicines* vol. 8 (12), 591. <https://doi.org/10.3390/biomedicines8120591>.
- Cabello, J., et al., 2014. PDR-1/hParkin negatively regulates the phagocytosis of apoptotic cell corpses in *Caenorhabditis elegans*. *Cell Death Dis.* vol. 5 (3) <https://doi.org/10.1038/cddis.2014.57>.
- Camacho, M., et al., 2021. Early constipation predicts faster dementia onset in Parkinson's disease. *NPJ Park. Dis.* vol. 7 (1), 45. <https://doi.org/10.1038/s41531-021-00191-w>.
- Camerucci, E., et al., 2023. Lifelong constipation in Parkinson's disease and other clinically defined alpha-synucleinopathies: a population-based study in Southeast Minnesota. *Parkinsonism Relat. Disord.* vol. 107, 105244 <https://doi.org/10.1016/j.parkreldis.2022.105244>.
- Chan, D., Citro, A., Cordy, J.M., Shen, G.C., Wolozin, B., 2011. Rac1 protein rescues neurite retraction caused by G2019s leucine-rich repeat kinase 2 (LRRK2). *J. Biol. Chem.* vol. 286 (18) <https://doi.org/10.1074/jbc.M111.234005>.
- Coppa, A., et al., 2020. The peroxisomal fatty acid transporter ABCD1/PMP-4 is required in the *C. elegans* hypodermis for axonal maintenance: a worm model for

- adrenoleukodystrophy. *Free Radic. Biol. Med.* vol. 152 <https://doi.org/10.1016/j.freeradbiomed.2020.01.177>.
- Dalfó, E., Ferrer, I., 2008. Early α -synuclein lipoxidation in neocortex in Lewy body diseases. *Neurobiol. Aging* vol. 29 (3), 408–417. <https://doi.org/10.1016/j.neurobiolaging.2006.10.022>.
- Ejsing, C.S., et al., 2009. Global analysis of the yeast lipidome by quantitative shotgun mass spectrometry. *Proc. Natl. Acad. Sci.* vol. 106 (7), 2136–2141. <https://doi.org/10.1073/pnas.0811700106>.
- Fanning, S., Selkoe, D., Dettmer, U., 2020. Parkinson's disease: proteinopathy or lipidopathy? *NPJ Parkinson's Dis.* vol. 6 (1), 3 <https://doi.org/10.1038/s41531-019-0103-7>.
- Feigin, V.L., et al., 2017. Global, regional, and national burden of neurological disorders during 1990–2015: a systematic analysis for the global burden of disease study 2015. *Lancet Neurol.* vol. 16 (11), 877–897. [https://doi.org/10.1016/S1474-4422\(17\)30299-5](https://doi.org/10.1016/S1474-4422(17)30299-5).
- Flowers, S., et al., 2023. Regulation of defective mitochondrial DNA accumulation and transmission in *C. elegans* by the programmed cell death and aging pathways. *Elife* vol. 12. <https://doi.org/10.7554/eLife.79725>.
- Fu, Y., et al., 2022. Increased unsaturated lipids underlie lipid peroxidation in synucleinopathy brain. *Acta Neuropathol. Commun.* vol. 10 (1), 165 <https://doi.org/10.1186/s40478-022-01469-7>.
- Gaig, C., Tolosa, E., 2009. When does Parkinson's disease begin? *Mov. Disord.* vol. 24 (S2), S656–S664. <https://doi.org/10.1002/mds.22672>.
- Gruntz, K., et al., 2018. Parkinson disease and the risk of epileptic seizures. *Ann. Neurol.* vol. 83 (2), 363–374. <https://doi.org/10.1002/ana.25157>.
- Hall, A., Lalli, G., 2010. Rho and Ras GTPases in Axon growth, guidance, and branching. *Cold Spring Harb. Perspect. Biol.* vol. 2 (2) <https://doi.org/10.1101/cshperspect.a001818>.
- Hamamichi, S., Rivas, R.N., Knight, A.L., Cao, S., Caldwell, K.A., Caldwell, G.A., 2008. Hypothesis-based RNAi screening identifies neuroprotective genes in a Parkinson's disease model. *Proc. Natl. Acad. Sci.* vol. 105 (2) <https://doi.org/10.1073/pnas.0711018105>.
- den Hartog Jager, W.A., 1969. Sphingomyelin in Lewy inclusion bodies in Parkinson's disease. *Arch. Neurol.* vol. 21 (6), 615–619. <https://doi.org/10.1001/archneur.1969.00480180071006>.
- Hinkle, J.T., Dawson, V.L., Dawson, T.M., 2019. The A1 astrocyte paradigm: new avenues for pharmacological intervention in neurodegeneration. *Mov. Disord.* vol. 34 (7), 959–969. <https://doi.org/10.1002/mds.27718>.
- Hou, N.S., et al., 2014. Activation of the endoplasmic reticulum unfolded protein response by lipid disequilibrium without disturbed proteostasis in vivo. *Proc. Natl. Acad. Sci.* vol. 111 (22) <https://doi.org/10.1073/pnas.1318262111>.
- Islimy, E., Girard, V., Gould, A.P., 2022. Functions of stress-induced lipid droplets in the nervous system. *Front. Cell Dev. Biol.* vol. 10 <https://doi.org/10.3389/fcell.2022.863907>.
- Kam, T.-I., Hinkle, J.T., Dawson, T.M., Dawson, V.L., 2020. Microglia and astrocyte dysfunction in parkinson's disease. *Neurobiol. Dis.* vol. 144, 105028 <https://doi.org/10.1016/j.nbd.2020.105028>.
- Kim, H., et al., 2018. The small GTPase RAC1/CED-10 is essential in maintaining dopaminergic neuron function and survival against α -synuclein-induced toxicity. *Mol. Neurobiol.* vol. 55 (9) <https://doi.org/10.1007/s12035-018-0881-7>.
- Kinchen, J.M., et al., 2005. Two pathways converge at CED-10 to mediate actin rearrangement and corpse removal in *C. elegans*. *Nature* vol. 434 (7029), 93–99. <https://doi.org/10.1038/nature03263>.
- Lee, S.-J., Zhang, J., Choi, A.M.K., Kim, H.P., 2013. Mitochondrial dysfunction induces formation of lipid droplets as a generalized response to stress. *Oxid. Med. Cell Longev.* 2013, 1–10. <https://doi.org/10.1155/2013/327167>.
- Lema, C., et al., 2020. 1H NMR serum metabolomic profiling of patients at risk of cardiovascular diseases performing stress test. *Sci. Rep.* vol. 10 (1), 17838 <https://doi.org/10.1038/s41598-020-74880-6>.
- Locke, C.J., Kautu, B.B., Berry, K.P., Lee, S.K., Caldwell, K.A., Caldwell, G.A., 2009. Pharmacogenetic analysis reveals a post-developmental role for Rac GTPases in *Caenorhabditis elegans* GABAergic neurotransmission. *Genetics* vol. 183 (4), 1357–1372. <https://doi.org/10.1534/genetics.109.106880>.
- Mahoney, T.R., et al., 2008. Intestinal signaling to GABAergic neurons regulates a rhythmic behavior in *Caenorhabditis elegans*. *Proc. Natl. Acad. Sci.* vol. 105 (42), 16350–16355. <https://doi.org/10.1073/pnas.0803617105>.
- Makasewicz, K., et al., 2021. Cooperativity of α -Synuclein binding to lipid membranes. *ACS Chem. Neurosci.* vol. 12 (12), 2099–2109. <https://doi.org/10.1021/acscchemneuro.1c00006>.
- Martínez-Arranz, I., et al., 2015. Enhancing metabolomics research through data mining. *J. Proteom.* vol. 127, 275–288. <https://doi.org/10.1016/j.jprote.2015.01.019>.
- Martínez-Sánchez, L. del C., et al., 2023. Epithelial RAC1-dependent cytoskeleton dynamics controls cell mechanics, cell shedding and barrier integrity in intestinal inflammation. *Gut* vol. 72 (2), 275–294. <https://doi.org/10.1136/gutjnl-2021-325520>.
- McIntire, S.L., Jorgensen, E., Horvitz, H.R., 1993. Genes required for GABA function in *Caenorhabditis elegans*. *Nature* vol. 364 (6435), 334–337. <https://doi.org/10.1038/364334a0>.
- Mew, M., Caldwell, K.A., Caldwell, G.A., 2022. From bugs to bedside: functional annotation of human genetic variation for neurological disorders using invertebrate models. *Hum. Mol. Genet.* vol. 31 (R1), R37–R46. <https://doi.org/10.1093/hmg/ddac203>.
- Murueta-Goyena, A., Andikotxea, A., Gómez-Esteban, J.C., Gabilondo, I., 2019. Contribution of the GABAergic system to non-motor manifestations in premotor and early stages of Parkinson's disease. *Front. Pharmacol.* vol. 10 <https://doi.org/10.3389/fphar.2019.01294>.
- Nargund, A.M., Pellegrino, M.W., Fiorese, C.J., Baker, B.M., Haynes, C.M., 2012. Mitochondrial import efficiency of ATFS-1 regulates mitochondrial UPR activation. *Science* vol. 337 (6094), 587–590. <https://doi.org/10.1126/science.1223560>.
- Nuzhnyi, E., et al., 2015. Plasma oligomeric Alpha-Synuclein is associated with Glucocerebrosidase activity in Gaucher disease. *Mov. Disord.* vol. 30 (7), 989–991. <https://doi.org/10.1002/mds.26200>.
- O'Rourke, E.J., Soukas, A.A., Carr, C.E., Ruvkun, G., 2009. *C. elegans* major fats are stored in vesicles distinct from Lysosome-Related organelles. *Cell Metab.* vol. 10 (5), 430–435. <https://doi.org/10.1016/j.cmet.2009.10.002>.
- Panicker, N., Ge, P., Dawson, V.L., Dawson, T.M., 2021. The cell biology of Parkinson's disease. *J. Cell Biol.* vol. 220 (4) <https://doi.org/10.1083/jcb.202012095>.
- Roussos, A., Kitopoulou, K., Borbolis, F., Palikaras, K., 2023. *Caenorhabditis elegans* as a model system to study human neurodegenerative disorders. *Biomolecules* vol. 13 (3), 478. <https://doi.org/10.3390/biom13030478>.
- Schapira, A.H.V., Chaudhuri, K.R., Jenner, P., 2017. Non-motor features of Parkinson disease. *Nat. Rev. Neurosci.* vol. 18 (7), 435–450. <https://doi.org/10.1038/nrn.2017.62>.
- Simonet, C., et al., 2022. Assessment of risk factors and early presentations of Parkinson disease in primary care in a diverse UK population. *JAMA Neurol.* vol. 79 (4), 359. <https://doi.org/10.1001/jamaneurol.2022.0003>.
- Stiernagle, T., 2006. Maintenance of *C. elegans*. *WormBook*. <https://doi.org/10.1895/wormbook.1.101.1>.
- Van Ham, T.J., Thijssen, K.L., Breitling, R., Hofstra, R.M.W., Plasterk, R.H.A., Nollen, E. A.A., 2008. *C. elegans* model identifies genetic modifiers of α -synuclein inclusion formation during aging. *PLOS Genet.* vol. 4 (3). <https://doi.org/10.1371/journal.pgen.1000027>.
- Winner, B., et al., 2011. In vivo demonstration that α -synuclein oligomers are toxic. *Proc. Natl. Acad. Sci.* vol. 108 (10), 4194–4199. <https://doi.org/10.1073/pnas.1100976108>.
- Yoneda, T., Benedetti, C., Urano, F., Clark, S.G., Harding, H.P., Ron, D., 2004. Compartment-specific perturbation of protein handling activates genes encoding mitochondrial chaperones. *J. Cell Sci.* vol. 117 (18), 4055–4066. <https://doi.org/10.1242/jcs.01275>.
- Yoo, D., Lim, Y., Son, Y., Rho, H., Shin, C., Ahn, T.-B., 2021. Dietary intake and plasma levels of polyunsaturated fatty acids in early-stage Parkinson's disease. *Sci. Rep.* vol. 11 (1), 12489 <https://doi.org/10.1038/s41598-021-92029-x>.
- Yu, Q.-J., et al., 2018. Parkinson disease with constipation: clinical features and relevant factors. *Sci. Rep.* vol. 8 (1), 567. <https://doi.org/10.1038/s41598-017-16790-8>.